

Fenton chemistry at aqueous interfaces

Shinichi Enami^{a,b,c,1}, Yosuke Sakamoto^d, and Agustín J. Colussi^{e,1}

^aThe Hakubi Center for Advanced Research, Kyoto University, Kyoto 606-8302, Japan; ^bResearch Institute for Sustainable Humanosphere, Kyoto University, Uji 611-0011, Japan; ^cPrecursory Research for Embryonic Science and Technology (PRESTO), Japan Science and Technology Agency, Kawaguchi 332-0012, Japan; ^dFaculty of Environmental Earth Science, Hokkaido University, Sapporo 060-0610, Japan; and ^eLinde Center for Global Environmental Science, California Institute of Technology, CA 91125

Edited by Richard J. Saykally, University of California, Berkeley, CA, and approved December 9, 2013 (received for review August 6, 2013)

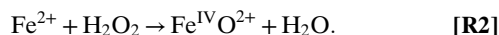
In a fundamental process throughout nature, reduced iron unleashes the oxidative power of hydrogen peroxide into reactive intermediates. However, notwithstanding much work, the mechanism by which Fe²⁺ catalyzes H₂O₂ oxidations and the identity of the participating intermediates remain controversial. Here we report the prompt formation of O=Fe^{IV}Cl₃⁻ and chloride-bridged di-iron O=Fe^{IV}·Cl·Fe^{II}Cl₄⁻ and O=Fe^{IV}·Cl·Fe^{III}Cl₅⁻ ferryl species, in addition to Fe^{III}Cl₄⁻, on the surface of aqueous FeCl₂ microjets exposed to gaseous H₂O₂ or O₃ beams for <50 μs. The unambiguous identification of such species in situ via online electrospray mass spectrometry let us investigate their individual dependences on Fe²⁺, H₂O₂, O₃, and H⁺ concentrations, and their responses to *tert*-butanol (an ·OH scavenger) and DMSO (an O-atom acceptor) cosolutes. We found that (i) mass spectra are not affected by excess *tert*-butanol, i.e., the detected species are primary products whose formation does not involve ·OH radicals, and (ii) the di-iron ferryls, but not O=Fe^{IV}Cl₃⁻, can be fully quenched by DMSO under present conditions. We infer that interfacial Fe(H₂O)_n²⁺ ions react with H₂O₂ and O₃ >10³ times faster than Fe(H₂O)₆²⁺ in bulk water via a process that favors inner-sphere two-electron O-atom over outer-sphere one-electron transfers. The higher reactivity of di-iron ferryls vs. O=Fe^{IV}Cl₃⁻ as O-atom donors implicates the electronic coupling of mixed-valence iron centers in the weakening of the Fe^{IV}-O bond in poly-iron ferryl species.

metal ions | reactive oxygen species | aerosols | advanced oxidation processes | nanoparticles

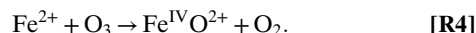
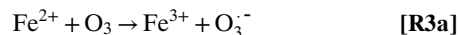
High-valent Fe^{IV}=O (ferryl) species participate in a wide range of key chemical and biological oxidations (1–4). Such species, along with ·OH radicals, have long been deemed putative intermediates in the oxidation of Fe^{II} by H₂O₂ (Fenton's reaction) (5, 6), O₃, or HOCl (7, 8). The widespread availability of Fe^{II} and peroxides in vivo (9–12), in natural waters and soils (13), and in the atmosphere (14–18) makes Fenton chemistry and Fe^{IV}=O groups ubiquitous features in diverse systems (19). A lingering issue regarding Fenton's reaction is how the relative yields of ferryls vs. ·OH radicals depend on the medium. For example, by assuming unitary ·OH radical yields, some estimates suggest that Fenton's reaction might account for ~30% of the ·OH radical production in fog droplets (20). Conversely, if Fenton's reaction mostly led to Fe^{IV}=O species, atmospheric chemistry models predict that their steady-state concentrations would be ~10⁴ times larger than [·OH], thereby drastically affecting the rates and course of oxidative chemistry in such media (20). Fe^{IV}=O centers are responsible for the versatility of the family of cytochrome P450 enzymes in catalyzing the oxidative degradation of a vast range of xenobiotics in vivo (21–28), and the selective functionalization of saturated hydrocarbons (29). The bactericidal action of antibiotics has been linked to their ability to induce Fenton chemistry in vivo (9, 30–34). Oxidative damage from exogenous Fenton chemistry likely is responsible for acute and chronic pathologies of the respiratory tract (35–38).

Despite its obvious importance, the mechanism of Fenton's reaction is not fully understood. What is at stake is how the coordination sphere of Fe²⁺ (39–46) under specific conditions affects the competition between the one-electron transfer

producing ·OH radicals (the Haber–Weiss mechanism) (47), reaction R1, and the two-electron oxidation via O-atom transfer (the Bray–Gorin mechanism) into Fe^{IV}O²⁺, reaction R2 (6, 23, 26, 27, 45, 48–51):



Ozone reacts with Fe²⁺ via analogous pathways leading to (formally) the same intermediates, reactions R3a, R3b, and R4 (8, 49, 52, 53):



At present, experimental evidence about these reactions is indirect, being largely based on the analysis of reaction products in bulk water in conjunction with various assumptions. Given the complex speciation of aqueous Fe²⁺/Fe³⁺ solutions, which includes diverse poly-iron species both as reagents and products, it is not surprising that classical studies based on the identification of reaction intermediates and products via UV-absorption spectra and the use of specific scavengers have fallen short of fully unraveling the mechanism of Fenton's reaction. Herein we address these issues, focusing particularly on the critically important interfacial Fenton chemistry that takes place at boundaries between aqueous and hydrophobic media, such as those

Significance

The Fenton reaction, Fe²⁺ + H₂O₂, plays fundamental roles in vivo and in advanced oxidation processes. Its mechanism and the identity of the intermediates involved, however, remain controversial. Here we present direct, mass-specific evidence of the prompt formation of mono- and poly-iron Fe^{IV}=O (ferryl) species on the surface of aqueous FeCl₂ microjets exposed to gaseous H₂O₂ or O₃ beams. Remarkably, Fe²⁺ ions at the aqueous surface react with H₂O₂ and O₃ >10³ times faster than Fe(H₂O)₆²⁺ in bulk water. Our results suggest that interfacial Fenton and Fenton-like chemistries could play a more significant role than hitherto envisioned.

Author contributions: S.E. designed research; S.E. and Y.S. performed research; S.E. contributed new reagents/analytic tools; S.E., Y.S., and A.J.C. analyzed data; and S.E. and A.J.C. wrote the paper.

The authors declare no conflict of interest.

This article is a PNAS Direct Submission.

Freely available online through the PNAS open access option.

¹To whom correspondence may be addressed. E-mail: enami.shinichi.3r@kyoto-u.ac.jp or ajcoluss@caltech.edu.

This article contains supporting information online at www.pnas.org/lookup/suppl/doi:10.1073/pnas.1314885111/-DCSupplemental.

present in atmospheric clouds (16), living tissues, biomembranes, bio-microenvironments (38, 54, 55), and nanoparticles (56, 57).

We exploited the high sensitivity, surface selectivity, and unambiguous identification capabilities of a newly developed instrument based on online electrospray mass spectrometry (ES-MS) (58–62) to identify the primary products of reactions **R1–R4** on aqueous FeCl_2 microjets exposed to gaseous H_2O_2 and O_3 beams under ambient conditions [in $\text{N}_2(\text{g})$ at 1 atm at $293 \pm 2 \text{ K}$]. Our experiments are conducted by intersecting the continuously refreshed, uncontaminated surfaces of free-flowing aqueous microjets with reactive gas beams for $\tau \sim 10\text{--}50 \mu\text{s}$, immediately followed (within $100 \mu\text{s}$; see below) by in situ detection of primary interfacial anionic products and intermediates via ES-MS (*Methods*, *SI Text*, and *Figs. S1* and *S2*). We have previously demonstrated that online mass spectrometric sampling of liquid microjets under ambient conditions is a surface-sensitive technique (58, 62–67).

Results and Discussion

Fig. 1 *A* and *B* shows negative ion ES mass spectra of the surface of $10 \mu\text{M}$ and $100 \mu\text{M}$ FeCl_2 aqueous microjets, respectively, while being exposed to $\text{O}_2(\text{g})$ and $\text{O}_3(\text{g})/\text{O}_2(\text{g})$ mixtures for contact times τ of the order of a few tens of microseconds. Gas-liquid contact times τ correspond to the estimated lifetimes of the microjets, i.e., before they are broken up by the nebulizer gas into submicrometer-sized droplets carrying net excess charges (58) (*SI Text*). A hard upper bound to τ can be derived from the

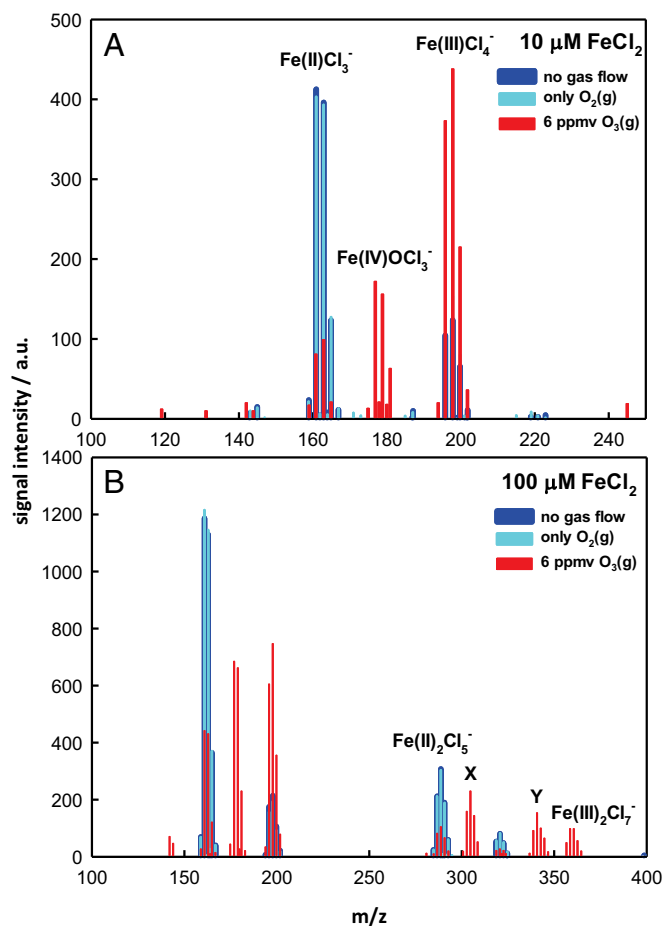


Fig. 1. Negative ion ES mass spectra of $10 \mu\text{M}$ (*A*) and $100 \mu\text{M}$ (*B*) FeCl_2 aqueous microjets exposed to $\text{O}_2(\text{g})$ or $\text{O}_3(\text{g})/\text{O}_2(\text{g})$ for $\sim 10\text{--}50 \mu\text{s}$. X and Y correspond to $\text{O}=\text{Fe}^{\text{IV}}\cdot\text{Cl}\cdot\text{Fe}^{\text{III}}\text{Cl}_4^-$ and $\text{O}=\text{Fe}^{\text{IV}}\cdot\text{Cl}\cdot\text{Fe}^{\text{III}}\text{Cl}_5^-$, respectively. See text for details.

fact that microdroplets carried by the nebulizer gas issuing from the injector nozzle at typical $v \sim 2 \times 10^4 \text{ cm}\cdot\text{s}^{-1}$ velocities would reach the inlet to the detection section of the mass spectrometer $\sim 2 \text{ cm}$ away from the tip of the nozzle in $< 100 \mu\text{s}$. The net charges produced during the aerodynamic breakup of the liquid jet represent the raw information acquired by the mass spectrometer (58). We confirmed experimentally that in our instrument charge separation among the anions and cations present in interfacial layers is largely driven pneumatically (rather than electrostatically/electrochemically) (68) by showing that signal intensities and anion fractionation increase at higher nebulizer gas velocities v and extrapolate to zero as $v \rightarrow 0$ (58). In Fig. 1*A*, the ES mass spectral multiplets at $m/z = 161, 163,$ and 165 correspond to $\text{Fe}^{\text{II}}\text{Cl}_3^-$. The characteristic multiplet patterns arising from natural abundance ^{35}Cl (75%) and ^{37}Cl (25%) chlorine isotopes let us establish the number of Cl^- contained in each detected species and, hence, the molecular composition of these singly charged ions (Fig. S3). In the presence of $\text{O}_3(\text{g})/\text{O}_2(\text{g})$ mixtures, new ES mass spectral clusters appear at $m/z = 177, 179,$ and 181 and $m/z = 196, 198,$ and 200 , which can be readily assigned to $\text{O}=\text{Fe}^{\text{IV}}\text{Cl}_3^-$ and $\text{Fe}^{\text{III}}\text{Cl}_4^-$, respectively. We verified that Cl^- is inert toward $\text{O}_3(\text{g})$ and does not participate in the oxidation process, in accord with the small value of $k(\text{Cl}^- + \text{O}_3) = 0.1 \text{ M}^{-1}\cdot\text{s}^{-1}$ in bulk water (69). Thus, $\sim 50\%$ Fe^{II} is oxidized by 6 parts per million by volume (ppmv) ($6 \times 10^{-6} \text{ atm}$) $\text{O}_3(\text{g})$ into Fe^{III} and Fe^{IV} at the air–water interface within $\tau \sim 10\text{--}50 \mu\text{s}$. This is a remarkable result because from (i) the (maximum) equilibrium concentration of dissolved O_3 in the experiments of Fig. 1— $[\text{O}_3(\text{aq})] = 6 \times 10^{-8} \text{ M}$ [from Henry's law constant for $\text{O}_3(\text{g})$ in bulk water at ambient temperature $H = 0.01 \text{ M atm}^{-1}$] (70)—and (ii) the rate coefficients of reactions **R3a**— $k_{3a} = (1.7 \pm 0.4) \times 10^5 \text{ M}^{-1}\cdot\text{s}^{-1}$ —and **R4**— $k_4 = (8.2 \pm 0.3) \times 10^5 \text{ M}^{-1}\cdot\text{s}^{-1}$ —in bulk water (7), we estimate that less than 0.1% Fe^{2+} should have been consumed under present conditions. In other words, reactions **R3a** and **R4** proceed $\sim 10^3\text{--}10^4$ times faster at the gas–water interface than in bulk water. The modest concentration enhancements of many gases at the air–water interface predicted by theoretical simulation (70) and demonstrated experimentally (71–74) would not substantially alter the above statement. We tentatively ascribe the significant acceleration of reaction **R4** at the gas–water interface to the enhanced lability and/or distorted geometry (75) of the hydration shell of Fe^{2+} at the interface relative to bulk water, a condition that would facilitate the substitution of O_3 for hydration waters and, hence, the direct interaction with the metal center required by O-atom transfer during subnanosecond gas–liquid encounters (76) (see below).

Fig. 1*B* shows additional peaks at higher masses. The ES mass signals at $m/z = 287, 289,$ and 291 correspond to $\text{Fe}^{\text{II}}_2\text{Cl}_5^-$. The group at $m/z = 303, 305,$ and 307 , hereafter labeled X, can be assigned to $\text{O}=\text{Fe}^{\text{IV}}\cdot\text{Cl}\cdot\text{Fe}^{\text{III}}\text{Cl}_4^-$ on the basis of peak masses and the characteristic Cl_5^- -multiplet pattern. Similarly, we assign the group at $m/z = 339, 341, 343, 345,$ and 347 , hereafter labeled Y, to $\text{O}=\text{Fe}^{\text{IV}}\cdot\text{Cl}\cdot\text{Fe}^{\text{III}}\text{Cl}_5^-$. Our results are qualitatively consistent with previous reports based on the UV-absorption detection of $\text{O}=\text{Fe}^{\text{IV}}$ species during the bulk ozonolysis of acidic Fe^{2+} (8, 23, 49, 52).

Fig. 2 *A–D* shows the evolution of reactant and products as functions of $[\text{O}_3(\text{g})]$ at FeCl_2 concentrations spanning the $1\text{--}1,000\text{-}\mu\text{M}$ range. It is apparent that although all signal intensities increase with $[\text{FeCl}_2]$, the ratio $\alpha = \text{O}=\text{Fe}^{\text{IV}}\text{Cl}_3^-/\text{Fe}^{\text{III}}\text{Cl}_4^-$ is not constant, as expected for the products of concurrent reactions **R3a** and **R4**, but both depend on $\text{O}_3(\text{g})$ and FeCl_2 concentrations (8, 51). It should be pointed out that mass signal intensities are not linear functions of bulk concentrations throughout, because the interfacial concentrations detected herein will plateau as the interface becomes saturated. Also, reactant signals may bottom out rather than vanish at sufficiently large $\text{O}_3(\text{g})$ [or $\text{H}_2\text{O}_2(\text{g})$] concentrations because interfacial layers are continuously replenished

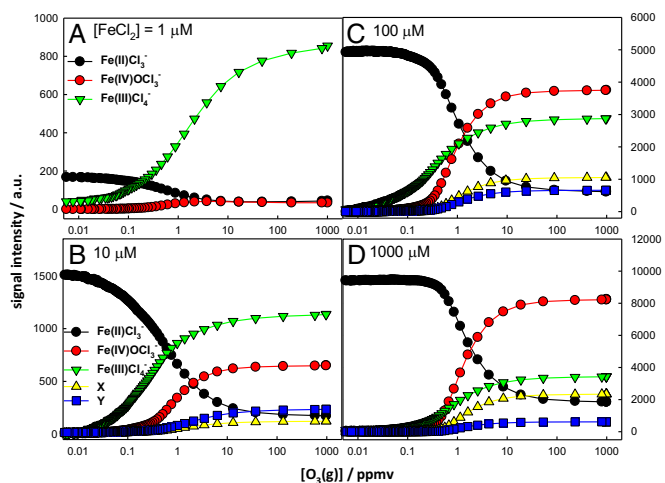
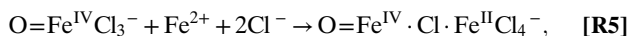


Fig. 2. ES mass spectral signal intensities of reactant and products at the surface of 1 μM (A), 10 μM (B), 100 μM (C), and 1,000 μM (D) FeCl_2 aqueous microjets as functions of the $\text{O}_3(\text{g})$ mixing ratio (1 ppmv = 2.5×10^{13} molecules per centimeter $^{-3}$ at 1 atm, 293 K). All experiments in 1 atm $\text{N}_2(\text{g})$ at 293 K. Background signal was subtracted for $\text{Fe}(\text{III})\text{Cl}_4^-$. X and Y correspond to $\text{O}=\text{Fe}^{\text{IV}}\cdot\text{Cl}\cdot\text{Fe}^{\text{III}}\text{Cl}_4^-$ and $\text{O}=\text{Fe}^{\text{IV}}\cdot\text{Cl}\cdot\text{Fe}^{\text{III}}\text{Cl}_5^-$, respectively.

by diffusion from the bulk liquid (66). Because the $\text{O}=\text{Fe}^{\text{IV}}\text{Cl}_3^-$ intermediate reacts further with Fe^{2+} via reaction **R5**,



the observed increase of α at higher $\text{O}_3(\text{g})$ and FeCl_2 concentrations is not the result of secondary chemistry (see below). Note that (i) the higher-mass products X, Y, and $\text{Fe}^{\text{III}}_2\text{Cl}_7^-$ appear at $[\text{FeCl}_2] \geq 10 \mu\text{M}$, and (ii) α depends weakly on pH (Fig. 3), in contrast to previous reports that $\text{O}=\text{Fe}^{\text{IV}}$ is formed only under very acidic (pH ≤ 2) bulk conditions (6, 8, 77). The more extensive hydrolysis of Fe^{2+} in more basic solutions prevented us from performing experiments above pH ~ 6.5 . It should be realized, however, that the acid–base properties of the air–water interface are quite different from those of bulk water. Whereas bulk water is neutral at pH 7, the aerial surface is neutral on bulk water at pH ~ 3.5 (63, 65, 78). This caveat prevents direct comparisons from being made between the pH-dependences observed herein and those previously reported for similar experiments in bulk solution. We wish to emphasize that the concentration dependences observed in our experiments strongly support our assumption that the detected species are produced on the surface of the intact jet (whose composition is identical to that of the injected solution) rather than on the ensemble of daughter droplets (whose compositions will span the broad distributions generated by random solvent evaporation) (63, 65) (see also *SI Text*).

We tested the effects of *tert*-butanol (*t*-BuOH) and DMSO additions to FeCl_2 microjets exposed to $\text{O}_3(\text{g})$. *t*-BuOH is an efficient scavenger of $\cdot\text{OH}$ radicals ($k_{\text{OH}+\textit{t}\text{-BuOH}} = 5 \times 10^8 \text{ M}^{-1}\cdot\text{s}^{-1}$ in bulk water) (79), whereas DMSO functions as both an $\cdot\text{OH}$ scavenger and an O-atom acceptor (6, 49, 52). Fig. 4 shows negative ion mass spectra of aqueous 100 μM FeCl_2 microjets containing large excesses ($100 \times [\text{FeCl}_2]$) of *t*-BuOH or DMSO upon exposure to $\text{O}_3(\text{g})$. Notably, the addition of *t*-BuOH has no effect whatsoever on mass spectra, thereby implying that $\cdot\text{OH}$ radicals do not participate in the formation of the observed products. Because $\cdot\text{OH}$ radicals, if present, also would react rapidly with Fe^{2+} [$k_{\text{OH}+\text{Fe}(\text{II})} = 3.2 \times 10^8 \text{ M}^{-1}\cdot\text{s}^{-1}$] (80) to produce more Fe^{3+} , we infer that the decomposition of their O_3^- precursor, reaction **R3b**, is too slow under present conditions.

The addition of DMSO as a cosolute, in contrast, has marked effects on product distribution. DMSO quenches most (but not all) ozonation products, such as $\text{O}=\text{Fe}^{\text{IV}}\cdot\text{Cl}\cdot\text{Fe}^{\text{II}}\text{Cl}_4^-$ and $\text{O}=\text{Fe}^{\text{IV}}\cdot\text{Cl}\cdot\text{Fe}^{\text{III}}\text{Cl}_5^-$, and all higher-mass poly-iron species. Remarkably, the mono-iron ferryl $\text{O}=\text{Fe}^{\text{IV}}\text{Cl}_3^-$ (and, as expected, $\text{Fe}^{\text{III}}\text{Cl}_4^-$) is not affected.

Similar experiments in which aqueous microjets containing 10 μM and 1 mM FeCl_2 , in the absence and presence of *t*-BuOH as a cosolute, were exposed to $\text{H}_2\text{O}_2(\text{g})/\text{N}_2(\text{g})$ mixtures led to the products shown in Fig. 5. A comparison of Figs. 1 and 5 confirms that H_2O_2 and O_3 react with interfacial Fe^{2+} along reactions **R1–R2** and **R3a,b–R4**, respectively, leading to (formally) the same products, albeit in different proportions. Note again that from Henry’s law constant for $\text{H}_2\text{O}_2(\text{g})$ in bulk water— $H = 10^5 \text{ M}\cdot\text{atm}^{-1}$ ($\sim 10^7$ times larger than for O_3) (81)—the maximum equilibrium concentration of dissolved H_2O_2 in the experiments of Fig. 5A is $[\text{H}_2\text{O}_2(\text{aq})] = 0.03 \text{ M}$. Therefore, from $k(\text{Fe}^{\text{II}} + \text{H}_2\text{O}_2) \sim 50 \text{ M}^{-1}\cdot\text{s}^{-1}$, we estimate that Fe^{2+} half-lives would be on the order of seconds if reactions **R1–R2** took place in bulk water, rather than a few tens of microseconds, as observed in our experiments (81). Note that in contrast to the O_3 case, $\text{O}=\text{Fe}^{\text{IV}}\text{Cl}_3^-$ is undetectable (compare Fig. 5 vis-a-vis Fig. 1), an event we ascribe to the slowness of **R2** relative to **R4** under present conditions, because $\text{O}=\text{Fe}^{\text{IV}}\text{Cl}_3^-$ would be consumed at the same rates via **R5** in both systems. We confirmed that the addition of DMSO as a cosolute in these experiments (Fig. S4) has an effect similar to those displayed in Fig. 4C.

The prompt formation of products in our experiments, at rates several orders of magnitude larger than those estimated for the same reactants dissolved in bulk water, and the peculiar variation in the ratio of the products of parallel reactions **R3a** and **R4** ($\text{Fe}^{\text{III}}\text{Cl}_4^-$ and $\text{O}=\text{Fe}^{\text{IV}}\text{Cl}_3^-$) as a function of ozone and Fe^{2+} concentrations reveal the exceptional characteristics of Fenton-like chemistry at the air–water interface. These phenomena, which could be typical of water–hydrophobe interfaces in general, reveal (i) the enhanced reactivity of interfacial Fe^{2+} as an O-atom acceptor from O_3 and H_2O_2 and (ii) the progressive emergence of such species to the outermost interfacial layers at higher Fe^{2+} bulk concentrations. Extensive ab initio molecular dynamics (Car–Parrinello) calculations that incorporate the water solvent explicitly would be required to elucidate the molecular details of these

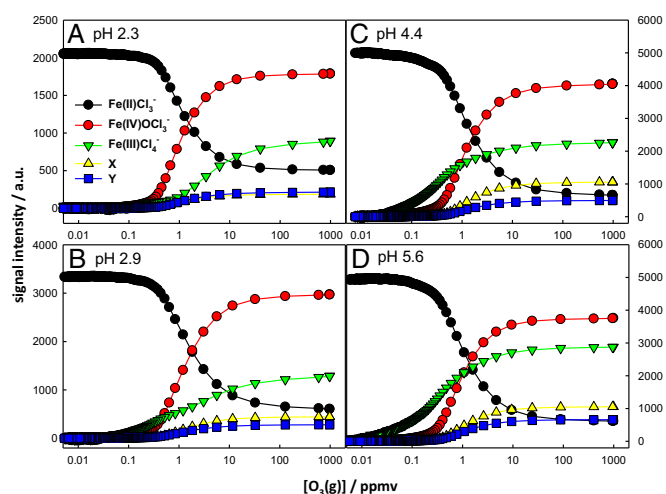


Fig. 3. ES mass spectral signal intensities of reactant and products from 100 μM FeCl_2 aqueous microjets at pH 2.3 (A), pH 2.9 (B), pH 4.4 (C), and pH 5.6 (D) as functions of the $\text{O}_3(\text{g})$ mixing ratio (1 ppmv = 2.5×10^{13} molecules per centimeter $^{-3}$ at 1 atm, 293 K). All experiments in 1 atm $\text{N}_2(\text{g})$ at 293 K. Background signal was subtracted for $\text{Fe}(\text{III})\text{Cl}_4^-$. X and Y correspond to $\text{O}=\text{Fe}^{\text{IV}}\cdot\text{Cl}\cdot\text{Fe}^{\text{II}}\text{Cl}_4^-$ and $\text{O}=\text{Fe}^{\text{IV}}\cdot\text{Cl}\cdot\text{Fe}^{\text{III}}\text{Cl}_5^-$, respectively.

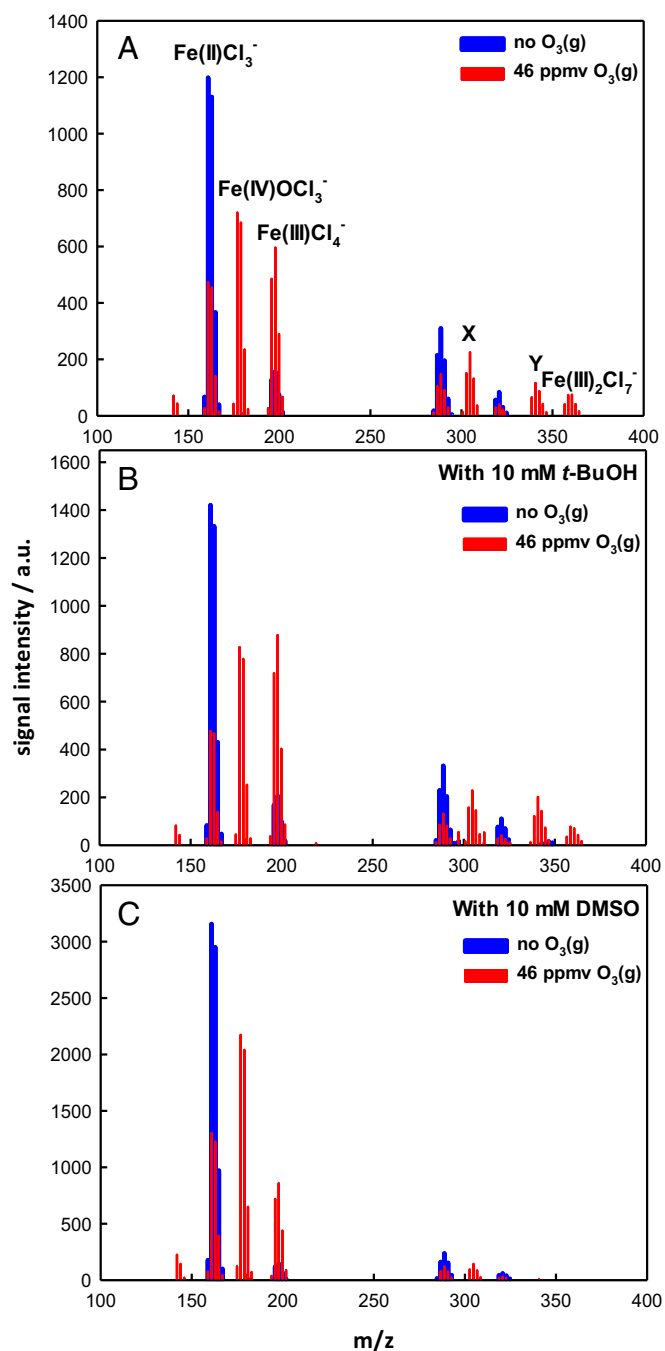


Fig. 4. Negative ion ES mass spectra of aqueous microjet containing 100 μM FeCl_2 in the absence (A) and presence (B) of 10 mM *t*-BuOH and in the presence of 10 mM DMSO (C), exposed to $\text{O}_3(\text{g})$ for ~ 10 – 50 μs . X and Y correspond to $\text{O}=\text{Fe}^{\text{IV}}\text{Cl}_3\text{Cl}_4^-$ and $\text{O}=\text{Fe}^{\text{IV}}\text{Cl}_3\text{Cl}_5^-$, respectively.

unique events at the gas–water interface (26, 48, 82). The possibility that doubly charged Fe^{2+} cations might be present in shallow interfacial layers is supported by molecular dynamics calculations, which predict that the concentration of doubly charged Mg^{2+} peaks at ~ 4 Å below the Gibbs dividing surface at values twice as large as its concentration in bulk water (83). Recent X-ray reflectivity studies confirmed the existence of nonmonotonic cation density profiles within ~ 1 -nm interfacial layers of aqueous electrolyte solutions (84). We cannot rule out the possibility that impinging gases are hydrated before colliding with the liquid surface (85, 86), but we deem it inconsequential because $\text{O}_3-(\text{H}_2\text{O})_n$ and

$\text{H}_2\text{O}_2-(\text{H}_2\text{O})_n$ complexes represent a very small fraction of O_3 and H_2O_2 gas flows under present conditions.

By considering that O-atom transfer, in contrast to electron transfer (reactions **R1** and **R3a**), requires direct contact of the O-atom donors (H_2O_2 and O_3) with the metal ion, and that the hydration waters of $\text{Fe}(\text{H}_2\text{O})_6^{2+}$ in bulk water are exchanged approximately every 0.5 μs (87), whereas $\text{O}_3(\text{g})$ remains trapped on the water surface for only 0.1 ns (76), our results imply that either (i) dissociative ligand substitution in interfacial $\text{Fe}(\text{H}_2\text{O})_6^{2+}$ (IF) is much faster than in $\text{Fe}(\text{H}_2\text{O})_6^{2+}$ in bulk water (B) or (ii) interfacial $\text{Fe}(\text{H}_2\text{O})_6^{2+}$ has a distorted octahedral geometry, on account of the broken symmetry, that lets O_3 approach the Fe^{2+} center via low-energy associative interchange pathways (88). Against this backdrop, our findings reveal that the dynamics and thermodynamics of ion hydration at aqueous interfaces are quite different from those in bulk water (75, 89). Thus, the roles and behavior of ions in many physical, chemical, and biological interfacial processes may not be predicted (or analyzed) from the properties of the corresponding ions in bulk water.

The dissimilar evolutions of $\text{O}=\text{Fe}^{\text{IV}}\text{Cl}_3^-$ and $\text{Fe}^{\text{III}}\text{Cl}_4^-$ in Figs. 2 and 3 are consistent with IF(z) depth profiles at the interface that depend on total $[\text{Fe}^{2+}]$. Everything happens as though the IF species involved in O-atom transfer are preferentially pushed to the surface of more concentrated Fe^{2+} solutions. In this context, it is relevant to point out that we recently found that hydronium (H_3O^+) emerges at the surface of water less than pH 4 as a “superacid” that protonates impinging gases having proton affinities larger than water (62, 64, 90). Thermodynamics dictates that this is possible only if interfacial H_3O^+ is weakly hydrated. If Fe^{2+} behaves similarly, the enhanced reactivity of IF relative to B and its emergence at the surface of more concentrated solutions could be alternatively ascribed to an incomplete hydration shell of IF.

We associate the significantly enhanced reactivity of poly-iron ferryls relative to $\text{O}=\text{Fe}^{\text{IV}}\text{Cl}_3^-$ as O-atom donors to DMSO with the weakening of the $\text{O}=\text{Fe}^{\text{IV}}$ bond, and ascribe such weakening to electronic rather than inductive effects. Our view is based on the fact that strong electron-donating ligands, such as thiolate (24), in the axial position are known to weaken and elongate the $\text{O}=\text{Fe}^{\text{IV}}$ bond in low-spin ($S = 1$) complexes by increasing the population of its σ - and π -antibonding molecular orbitals (45). Because a Cl^- ligand coordinatively bound to Fe^{II} (as in X) or Fe^{III} (as in Y) should be less nucleophilic than unbound Cl^- , the enhanced reactivity of poly-iron ferryls appears to be a result of

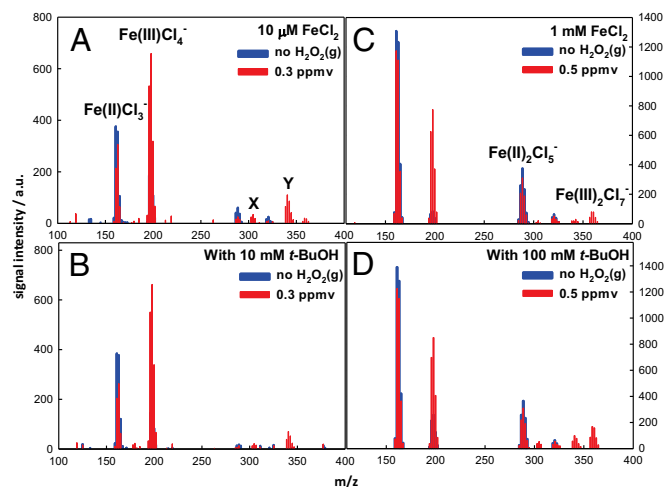


Fig. 5. Negative ion ES mass spectra of 10 μM (A and B) and 1 mM (C and D) FeCl_2 aqueous microjets in the absence/presence of excess *t*-BuOH as a cosolute exposed to $\text{H}_2\text{O}_2(\text{g})$ for ~ 10 – 50 μs . X and Y correspond to $\text{O}=\text{Fe}^{\text{IV}}\text{Cl}_3\text{Cl}_4^-$ and $\text{O}=\text{Fe}^{\text{IV}}\text{Cl}_3\text{Cl}_5^-$, respectively.

the electronic coupling of the iron centers via Cl^- bridges. Further experimental work and high-level quantum chemistry calculations are needed to fully elucidate the molecular basis of the O-donating power of poly-iron ferryls.

In summary, we present compelling evidence of the prompt formation of mono- and poly-iron Fe^{IV} species on the surface of aqueous $\text{Fe}^{\text{II}}\text{Cl}_2$ microjets exposed to gaseous H_2O_2 or O_3 beams. The exceedingly fast reactions of interfacial Fe^{2+} with gas-phase H_2O_2 and O_3 [10^3 – 10^4 times faster than similar reactions of $\text{Fe}(\text{H}_2\text{O})_6^{2+}$ in bulk aqueous media] are ascribed to a labile/incomplete hydration shell that favors inner-sphere O-atom transfers over outer-sphere one-electron transfers. The finding that di-iron ferryls $\text{O}=\text{Fe}^{\text{IV}}\cdot\text{Cl}\cdot\text{Fe}^{\text{IV}}\text{Cl}_4^-$ and $\text{O}=\text{Fe}^{\text{IV}}\cdot\text{Cl}\cdot\text{Fe}^{\text{III}}\text{Cl}_5^-$ are fully scavenged by the O-atom acceptor DMSO, whereas $\text{O}=\text{Fe}^{\text{IV}}\text{Cl}_3^-$ is not, implicates the electronic coupling of mixed-valence iron centers in weakening the $\text{Fe}^{\text{IV}}=\text{O}$ bond. Present results suggest a more significant role than hitherto envisioned for the Fe^{IV} species produced in Fenton and Fenton-like chemistries at aqueous interfaces opposite hydrophobic media, such as air in atmospheric aerosols and clouds, proteins in living tissues, bio-membranes, and bio-microenvironments.

Methods

Our experiments involve the injection of aqueous FeCl_2 jets into the spraying chamber of an ES mass spectrometer (Agilent 6130 Quadrupole LC/MS Electrospray System) flushed with $\text{N}_2(\text{g})$ at 1 atm, 293 K. Jets are exposed therein to orthogonal gas-phase O_3 or H_2O_2 beams. The species produced on the surface of such jets are analyzed in situ via online ES-MS. The present experimental setup essentially is the same as the one reported elsewhere (62, 64, 65). Solutions are pumped ($100\ \mu\text{L}\cdot\text{min}^{-1}$) into the spraying chamber through a grounded stainless steel needle ($100\text{-}\mu\text{m}$ bore) coaxial with a sheath-issuing nebulizer $\text{N}_2(\text{g})$ at a high gas velocity v_g ($\sim 160\ \text{m/s}$). The species detected by ES-MS are assumed to be produced in collisions of gaseous H_2O_2 or O_3 with the surface of the intact aqueous jets containing microdroplets ($D_0 > 1\ \mu\text{m}$) as they emerge from the nozzle, i.e., before they are broken up into submicrometer-sized droplets (58) (see also *SI Text*). These smaller droplets already carry net charge of either sign. It should be

emphasized that charge separation is a one-time event driven by the conversion of kinetic energy of the nebulizer gas into surface and electrostatic energies of submicrometer-sized droplets (58). We have demonstrated the surface specificity of our experiments by showing that (i) anion signal intensities in the mass spectra of equimolar salt solutions adhere to a normal Hofmeister series (rather than being identical) (91, 92), (ii) the depth of the interfacial layers sampled is controllable as a function of nebulizer gas velocity v (58), and (iii) they allow the detection of products of gas–liquid reactions that could be formed only at the air–water interface (62, 64–66, 71).

Gaseous hydrogen peroxide, $\text{H}_2\text{O}_2(\text{g})$, was injected into the spraying chamber carried by ultrapure ($>99.999\%$) $\text{N}_2(\text{g})$ sparging hydrogen peroxide solution [extra pure reagent, 30% (wt/wt) in water; Nacalai Tesque] kept in a trap held at 293 K in a temperature-controlled bath (TRC-4C; Thomas). Carrier gas flow rates were regulated by calibrated digital mass flow controllers (SEC-400 Mark 3; Horiba STEC) up to 1 standard liter per minute (Fig. S1). [$\text{H}_2\text{O}_2(\text{g})$] was derived from the reported H_2O_2 vapor pressures of H_2O_2 : H_2O mixture at the temperatures (93). We verified that Cl^- is inert toward $\text{H}_2\text{O}_2(\text{g})$ under present conditions (Fig. S5). Teflon gas lines were cleaned and dried daily with ultrapure nitrogen gas. Ozone was generated by flowing ultrapure $\text{O}_2(\text{g})$ ($>99.998\%$; Kyoto Teisan) through a silent discharge ozonizer (KSQ-050; Kotohira) and quantified via online UV-visible absorption spectrophotometry (Agilent 8453; Agilent Technologies) at 250 and 300 nm [absorption cross sections $\sigma(250\ \text{nm}) = 1.1 \times 10^{-17}$, $\sigma(300\ \text{nm}) = 3.9 \times 10^{-19}\ \text{cm}^2\cdot\text{molecule}^{-1}$ at 298 K] before entering the reaction chamber (Fig. S2). Throughout, the reported [$\text{O}_3(\text{g})$] values, which correspond to the concentrations actually sensed by the microjets in the reaction chamber, are estimated to be ~ 13 times smaller than the values determined from UV absorbance because of further dilution by the drying gas. The gas molecule hitting the surface of the pH-adjusted (by concentrated HCl/NaOH , and the pH was already measured by a calibrated pH meter, Horiba LAQUA F-74, before the experiments) aqueous microjet can stick to it by accommodation, reacting therein, or rebound (94, 95). See *Supporting Information* for more details.

ACKNOWLEDGMENTS. We are grateful to Dr. Himanshu Mishra and Profs. Michael Hoffmann, William Goddard, and Harry Gray of the California Institute of Technology for valuable discussions. S.E. thanks the Japan Science and Technology Agency PRESTO program, Grant for Environmental Research Projects from The Sumitomo Foundation, and Steel Foundation for Environmental Protection Technology. Y.S. thanks the Grant-in-Aid for Japan Society for the Promotion of Science Fellows for financial support.

1. Groves JT (2006) High-valent iron in chemical and biological oxidations. *J Inorg Biochem* 100(4):434–447.
2. Sheldon RA, Kochi JK (1981) *Metal-Catalyzed Oxidation of Organic Compounds* (Academic, New York).
3. Bakac A (2010) Oxygen activation with transition-metal complexes in aqueous solution. *Inorg Chem* 49(8):3584–3593.
4. Lemire JA, Harrison JJ, Turner RJ (2013) Antimicrobial activity of metals: Mechanisms, molecular targets and applications. *Nat Rev Microbiol* 11(6):371–384.
5. Fenton HJH (1894) Oxidation of tartaric acid in presence of iron. *J Chem Soc Trans* 65:899–910.
6. Bataineh H, Pestovsky O, Bakac A (2012) pH-induced mechanistic changeover from hydroxyl radicals to iron(IV) in the Fenton reaction. *Chem. Sci.* 3(5):1594–1599.
7. Conocchioli TJ, Hamilton EJ, Sutin N (1965) Formation of iron(IV) in the oxidation of iron(II). *J Am Chem Soc* 87(4):926–927.
8. Logager T, Holcman J, Sehested K, Pedersen T (1992) Oxidation of ferrous-ions by ozone in acidic solutions. *Inorg Chem* 31(17):3523–3529.
9. Kohanski MA, Dwyer DJ, Hayete B, Lawrence CA, Collins JJ (2007) A common mechanism of cellular death induced by bactericidal antibiotics. *Cell* 130(5):797–810.
10. Mishra S, Imlay J (2012) Why do bacteria use so many enzymes to scavenge hydrogen peroxide? *Arch Biochem Biophys* 525(2):145–160.
11. Rouault TA (2009) Cell biology. An ancient gauge for iron. *Science* 326(5953):676–677.
12. Rhee SG (2006) Cell signaling. H_2O_2 , a necessary evil for cell signaling. *Science* 312(5782):1882–1883.
13. Lee C, et al. (2008) Bactericidal effect of zero-valent iron nanoparticles on *Escherichia coli*. *Environ Sci Technol* 42(13):4927–4933.
14. Harris E, et al. (2013) Enhanced role of transition metal ion catalysis during in-cloud oxidation of SO_2 . *Science* 340(6133):727–730.
15. Charrier JG, Anastasio C (2011) Impacts of antioxidants on hydroxyl radical production from individual and mixed transition metals in a surrogate lung fluid. *Atmos Environ* 45(40):7555–7562.
16. Deguillaume L, et al. (2005) Transition metals in atmospheric liquid phases: Sources, reactivity, and sensitive parameters. *Chem Rev* 105(9):3388–3431.
17. Jacob DJ (2000) Heterogeneous chemistry and tropospheric ozone. *Atmos Environ* 34(12–14):2131–2159.
18. Seinfeld JH, Pandis SN (2006) *Atmospheric Chemistry and Physics: From Air Pollution to Climate Change* (Wiley, Hoboken, NJ), 2nd Ed.
19. Dunford HB (2002) Oxidations of iron(II)/(III) by hydrogen peroxide: From aquo to enzyme. *Coord Chem Rev* 233:311–318.
20. Deguillaume L, Leriche M, Chaumerliac N (2005) Impact of radical versus non-radical pathway in the Fenton chemistry on the iron redox cycle in clouds. *Chemosphere* 60(5):718–724.
21. Cho KB, et al. (2012) Evidence for an alternative to the oxygen rebound mechanism in C-H bond activation by non-heme Fe(IV)O complexes. *J Am Chem Soc* 134(50):20222–20225.
22. Prat I, et al. (2011) Observation of Fe(V)=O using variable-temperature mass spectrometry and its enzyme-like C-H and C=C oxidation reactions. *Nat Chem* 3(10):788–793.
23. Pestovsky O, Bakac A (2004) Reactivity of aqueous Fe(IV) in hydride and hydrogen atom transfer reactions. *J Am Chem Soc* 126(42):13757–13764.
24. Green MT, Dawson JH, Gray HB (2004) Oxoiron(IV) in chloroperoxidase compound II is basic: Implications for P450 chemistry. *Science* 304(5677):1653–1656.
25. Munro AW, Girvan HM, Mason AE, Dunford AJ, McLean KJ (2013) What makes a P450 tick? *Trends Biochem Sci* 38(3):140–150.
26. Ensing B, Buda F, Gribnau MCM, Baerends EJ (2004) Methane-to-methanol oxidation by the hydrated iron(IV) oxo species in aqueous solution: A combined DFT and Car-Parrinello molecular dynamics study. *J Am Chem Soc* 126(13):4355–4365.
27. Decker A, et al. (2007) Spectroscopic and quantum chemical studies on low-spin $\text{Fe}^{\text{IV}}=\text{O}$ complexes: Fe-O bonding and its contributions to reactivity. *J Am Chem Soc* 129(51):15983–15996.
28. Srncic M, Wong SD, England J, Que L, Jr., Solomon EI (2012) π -Frontier molecular orbitals in S = 2 ferryl species and elucidation of their contributions to reactivity. *Proc Natl Acad Sci USA* 109(36):14326–14331.
29. Barton DHR, Doller D (1992) The selective functionalization of saturated hydrocarbons—Gif chemistry. *Acc Chem Res* 25(11):504–512.
30. Yeom J, Imlay JA, Park W (2010) Iron homeostasis affects antibiotic-mediated cell death in *Pseudomonas* species. *J Biol Chem* 285(29):22689–22695.
31. Juárez-Hernández RE, Miller PA, Miller MJ (2012) Syntheses of siderophore-drug conjugates using a convergent thiol-maleimide system. *ACS Med Chem Lett* 3(10):799–803.
32. Freinbichler W, et al. (2011) Highly reactive oxygen species: Detection, formation, and possible functions. *Cell Mol Life Sci* 68(12):2067–2079.
33. Keren I, Wu YX, Inocencio J, Mulcahy LR, Lewis K (2013) Killing by bactericidal antibiotics does not depend on reactive oxygen species. *Science* 339(6124):1213–1216.
34. Luo YZ, Han ZX, Chin SM, Linn S (1994) Three chemically distinct types of oxidants formed by iron-mediated Fenton reactions in the presence of DNA. *Proc Natl Acad Sci USA* 91(26):12438–12442.

35. Akatsuka S, et al. (2012) Fenton reaction induced cancer in wild type rats recapitulates genomic alterations observed in human cancer. *PLoS One* 7(8):e43403.
36. Jiang L, et al. (2012) Iron overload signature in chrysotile-induced malignant mesothelioma. *J Pathol* 228(3):366–377.
37. Jomova K, Baros S, Valko M (2012) Redox active metal-induced oxidative stress in biological systems. *Transit Met Chem* 37(2):127–134.
38. Wang B, et al. (2013) Physicochemical origin for free radical generation of iron oxide nanoparticles in biomicroenvironment: Catalytic activities mediated by surface chemical states. *J Phys Chem C* 117(11):383–392.
39. Bernasconi L, Baerends EJ (2008) The EDTA complex of oxidoiron(IV) as realisation of an optimal ligand environment for high activity of FeO^{2+} . *Eur J Inorg Chem* 2008(10): 1672–1681.
40. Latifi R, Sainna MA, Rybak-Akimova EV, de Visser SP (2013) Does hydrogen-bonding donation to manganese(IV)-oxo and iron(V)-oxo oxidants affect the oxygen-atom transfer ability? A computational study. *Chemistry* 19(12):4058–4068.
41. Ye SF, Geng CY, Shaik S, Neese F (2013) Electronic structure analysis of multistate reactivity in transition metal catalyzed reactions: The case of C-H bond activation by non-heme iron(IV)-oxo cores. *Phys Chem Chem Phys* 15(21):8017–8030.
42. Schwarz H (2011) Chemistry with methane: Concepts rather than recipes. *Angew Chem Int Ed Engl* 50(43):10096–10115.
43. Fu Q, et al. (2010) Interface-confined ferrous centers for catalytic oxidation. *Science* 328(5982):1141–1144.
44. McDonald AR, Que L (2013) High-valent nonheme iron-oxo complexes: Synthesis, structure, and spectroscopy. *Coord Chem Rev* 257(2):414–428.
45. Jackson TA, et al. (2008) Axial ligand effects on the geometric and electronic structures of nonheme oxoiron(IV) complexes. *J Am Chem Soc* 130(37):12394–12407.
46. Hofstetter TE, Armentrout PB (2013) Threshold collision-induced dissociation and theoretical studies of hydrated Fe(II): Binding energies and Coulombic barrier heights. *J Phys Chem A* 117(6):1110–1123.
47. Weiss J (1934) Reaction mechanism of oxidation-reduction processes. *Nature* 133: 648–649.
48. Ensing B, Buda F, Blöchl P, Baerends EJ (2001) Chemical Involvement of Solvent Water Molecules in Elementary Steps of the Fenton Oxidation Reaction. *Angew Chem Int Ed Engl* 40(15):2893–2895.
49. Pestovsky O, Bakac A (2006) Aqueous ferryl(IV) ion: Kinetics of oxygen atom transfer to substrates and oxo exchange with solvent water. *Inorg Chem* 45(2):814–820.
50. Kremer ML (1999) Mechanism of the Fenton reaction. Evidence for a new intermediate. *Phys Chem Chem Phys* 1(15):3595–3605.
51. Bossmann SH, et al. (1998) New evidence against hydroxyl radicals as reactive intermediates in the thermal and photochemically enhanced Fenton reactions. *J Phys Chem A* 102(28):5542–5550.
52. Pestovsky O, et al. (2005) Aqueous Fe-IV=O: Spectroscopic identification and oxo-growth exchange. *Angew Chem Int Ed* 44(42):6871–6874.
53. Sakamoto Y, Enami S, Tonokura K (2013) Enhancement of gaseous iodine emission by aqueous ferrous ions during the heterogeneous reaction of gaseous ozone with aqueous iodide. *J Phys Chem A* 117(14):2980–2986.
54. Terman A, Kurz T (2013) Lysosomal iron, iron chelation, and cell death. *Antioxid Redox Signal* 18(8):888–898.
55. Watt RK (2013) A unified model for ferritin iron loading by the catalytic center: implications for controlling “free iron” during oxidative stress. *ChemBioChem* 14(4): 415–419.
56. Dhakshinamoorthy A, Navalon S, Alvaro M, Garcia H (2012) Metal nanoparticles as heterogeneous Fenton catalysts. *ChemSusChem* 5(1):46–64.
57. Wang JL, Xu LJ (2012) Advanced oxidation processes for wastewater treatment: Formation of hydroxyl radical and application. *Crit Rev Environ Sci Technol* 42(3): 251–325.
58. Enami S, Colussi AJ (2013) Long-range specific ion-ion interactions in hydrogen-bonded liquid films. *J Chem Phys* 138(18):184706.
59. Enami S, Mishra H, Hoffmann MR, Colussi AJ (2012) Hofmeister effects in micromolar electrolyte solutions. *J Chem Phys* 136(15):154707.
60. Mollah S, Pris AD, Johnson SK, Gwizdala AB, Houk RS (2000) Identification of metal cations, metal complexes, and anions by electrospray mass spectrometry in the negative ion mode. *Anal Chem* 72(5):985–991.
61. Enami S, Colussi AJ (2013) Long-range Hofmeister effects of anionic and cationic amphiphiles. *J Phys Chem B* 117(20):6276–6281.
62. Enami S, Hoffmann MR, Colussi AJ (2012) Dry deposition of biogenic terpenes via cationic oligomerization on environmental aqueous surfaces. *J Phys Chem Lett* 3(21): 3102–3108.
63. Mishra H, et al. (2012) Bronsted basicity of the air-water interface. *Proc Natl Acad Sci USA* 109(46):18679–18683.
64. Enami S, Stewart LA, Hoffmann MR, Colussi AJ (2010) Superacid chemistry on mildly acidic water. *J Phys Chem Lett* 1(24):3488–3493.
65. Enami S, Hoffmann MR, Colussi AJ (2010) Proton availability at the air/water interface. *J Phys Chem Lett* 1(10):1599–1604.
66. Enami S, Hoffmann MR, Colussi AJ (2008) Acidity enhances the formation of a persistent ozonide at aqueous ascorbate/ozone gas interfaces. *Proc Natl Acad Sci USA* 105(21):7365–7369.
67. Mishra H, et al. (2012) Anions dramatically enhance proton transfer through aqueous interfaces. *Proc Natl Acad Sci USA* 109(26):10228–10232.
68. Zilch LW, Maze JT, Smith JW, Ewing GE, Jarrold MF (2008) Charge separation in the aerodynamic breakup of micrometer-sized water droplets. *J Phys Chem A* 112(51): 13352–13363.
69. Enami S, Vecitis CD, Cheng J, Hoffmann MR, Colussi AJ (2007) Global inorganic source of atmospheric bromine. *J Phys Chem A* 111(36):8749–8752.
70. Vacha R, Slavicek P, Mucha M, Finlayson-Pitts BJ, Jungwirth P (2004) Adsorption of atmospherically relevant gases at the air/water interface: Free energy profiles of aqueous solvation of N_2 , O_2 , O_3 , OH, H_2O , HO_2 , and H_2O_2 . *J Phys Chem A* 108(52): 11573–11579.
71. Enami S, Hoffmann MR, Colussi AJ (2010) Prompt formation of organic acids in pulse ozonation of terpenes on aqueous surfaces. *J Phys Chem Lett* 1(15):2374–2379.
72. Finlayson-Pitts BJ (2009) Reactions at surfaces in the atmosphere: Integration of experiments and theory as necessary (but not necessarily sufficient) for predicting the physical chemistry of aerosols. *Phys Chem Chem Phys* 11(36):7760–7779.
73. Donaldson DJ, Valsaraj KT (2010) Adsorption and reaction of trace gas-phase organic compounds on atmospheric water film surfaces: a critical review. *Environ Sci Technol* 44(3):865–873.
74. Shiraiwa M, et al. (2011) The role of long-lived reactive oxygen intermediates in the reaction of ozone with aerosol particles. *Nat Chem* 3(4):291–295.
75. Meng S, Chakarov DV, Kasemo B, Gao SW (2004) Two-dimensional hydration shells of alkali metal ions at a hydrophobic surface. *J Chem Phys* 121(24):12572–12576.
76. Roeselova M, Jungwirth P, Tobias DJ, Gerber RB (2003) Impact, trapping, and accommodation of hydroxyl radical and ozone at aqueous salt aerosol surfaces. A molecular dynamics study. *J Phys Chem B* 107(46):12690–12699.
77. Hug SJ, Leupin O (2003) Iron-catalyzed oxidation of arsenic(III) by oxygen and by hydrogen peroxide: pH-dependent formation of oxidants in the Fenton reaction. *Environ Sci Technol* 37(12):2734–2742.
78. Saykally RJ (2013) Air/water interface: Two sides of the acid-base story. *Nat Chem* 5(2): 82–84.
79. Staehelin J, Hoigne J (1985) Decomposition of ozone in water in the presence of organic solutes acting as promoters and inhibitors of radical chain reactions. *Environ Sci Technol* 19(12):1206–1213.
80. De Laat J, Gallard H (1999) Catalytic decomposition of hydrogen peroxide by Fe(III) in homogeneous aqueous solution: Mechanism and kinetic modeling. *Environ Sci Technol* 33(16):2726–2732.
81. Finlayson-Pitts BJ, Pitts JN (2000) *Chemistry of the Upper and Lower Atmosphere* (Academic, San Diego, CA).
82. Louwerse MJ, Vassilev P, Baerends EJ (2008) Oxidation of methanol by FeO^{2+} in water: DFT calculations in the gas phase and ab initio MD simulations in water solution. *J Phys Chem A* 112(5):1000–1012.
83. Callahan KM, et al. (2010) Effect of magnesium cation on the interfacial properties of aqueous salt solutions. *J Phys Chem A* 114(32):8359–8368.
84. Luo G, et al. (2013) X-ray reflectivity reveals a nonmonotonic ion-density profile perpendicular to the surface of ErCl_3 aqueous solutions. *J Phys Chem C* 117(37): 19082–19090.
85. Vaida V (2011) Perspective: Water cluster mediated atmospheric chemistry. *J Chem Phys* 135(2):020901.
86. Buszek RJ, Francisco JS, Anglada JM (2011) Water effects on atmospheric reactions. *Int Rev Phys Chem* 30(3):335–369.
87. Kerisit S, Rosso KM (2009) Transition path sampling of water exchange rates and mechanisms around aqueous ions. *J Chem Phys* 131(11):114512.
88. Rotzinger FP (1997) Mechanism of water exchange for the di- and trivalent metal hexaaqua ions of the first transition series. *J Am Chem Soc* 119(22):5230–5238.
89. Cheng YK, Rossy PJ (1998) Surface topography dependence of biomolecular hydrophobic hydration. *Nature* 392(6677):696–699.
90. Enami S, Mishra H, Hoffmann MR, Colussi AJ (2012) Protonation and oligomerization of gaseous isoprene on mildly acidic surfaces: Implications for atmospheric chemistry. *J Phys Chem A* 116(24):6027–6032.
91. Cheng J, Hoffmann MR, Colussi AJ (2008) Anion fractionation and reactivity at air/water:methanol interfaces. Implications for the origin of Hofmeister effects. *J Phys Chem B* 112(24):7157–7161.
92. Cheng J, Vecitis CD, Hoffmann MR, Colussi AJ (2006) Experimental anion affinities for the air/water interface. *J Phys Chem B* 110(51):25598–25602.
93. Hwang H, Dasgupta PK (1985) Thermodynamics of the hydrogen peroxide-water system. *Environ Sci Technol* 19(3):255–258.
94. Dempsey LP, Brastad SM, Nathanson GM (2011) Interfacial acid dissociation and proton exchange following collisions of DCl with salty glycerol and salty water. *J Phys Chem Lett* 2(6):622–627.
95. Davidovits P, Kolb CE, Williams LR, Jayne JT, Worsnop DR (2006) Mass accommodation and chemical reactions at gas-liquid interfaces. *Chem Rev* 106(4):1323–1354.